Low loss GaInNAs/GaAs gain waveguides with U-bend geometry for single-facet coupling in hybrid photonic integration

Low loss GaInNAs/GaAs gain waveguides with U-bend geometry for single-facet coupling in hybrid photonic integration

Heidi Tuorila,[1] Jukka Viheriälä,[1] Matteo Cherchi,[2] Antti T. Aho,[1] Timo Aalto,[2] Mircea Guina[1]

[1] Optoelectronics Research Centre, Tampere University of Technology, 33101 Tampere, Finland
[2] VTT Technical Research Centre of Finland, Espoo 02044, Finland

We report a low loss U-bend waveguide for realization of GaAs-based gain elements employed in hybrid photonic integration. This architecture allows to position the input and output ports of the gain waveguide on the same facet and thus alleviates the geometrical constrains in hybrid integration, i.e. the need for precise alignment with silicon photonics waveguides on both ends of the III-V chip. As an exemplary demonstration, we report the loss and gain characteristics of GaInNAs/GaAs U-bend waveguides operating at 1.3 μm. In particular, we demonstrate a bending loss as low as 1.1 dB for an 83 μm bending radius. Efficient laser diode operation is also demonstrated.

Silicon photonics has gained tremendous success over the past years due to its ability to provide a robust, miniaturized and relatively low-loss integration platform for photonics. Silicon, however, lacks the ability to provide optical gain, for example to generate light or to compensate for coupling and propagation losses. The most mature approaches to add gain to the silicon platform rely on III-V materials that can be combined using hybrid, heterogeneous, or monolithic integration[1]. Heterogeneous and monolithic integration ensure a good alignment of the silicon waveguides and the III-V elements, owing to the use of high precision stepper lithography. On the other hand, they require dedicated, non-conventional fabrication lines, as III-V materials are not compatible with standard CMOS lines. Therefore, these two approaches ruin one of the main arguments in favor of the silicon photonics, i.e. the CMOS compatibility, and become economically viable only for very large volume production. On the other hand, hybrid integration appears to provide the flexibility in customizing application specific photonic integrated circuits (PICs), in particular for lower volumes, but could also fulfill the needs for large volume fabrication once simpler and automated integration processes are deployed.

Here we address the need for advanced approaches enabling a more efficient and simplified coupling between the III-V and passive PIC waveguides. In particular, we focus on a design targeting travelling-wave semiconductor optical amplifiers (TW-SOAs). In general, the proposed design can be used to realize other III-V-based waveguide devices, such as laser diodes and electro-absorption modulators, which are instrumental for silicon-based PIC technology, for example employing silicon on insulator (SOI) μm-scale waveguides[2]. In this case, the integration scheme is based on flip-chip bonding of the III-V chip onto a recessed area of SOI wafer and butt-coupling between the waveguides on Si and the III-V chip[3], as shown in the example of Figure 1 (a). Even

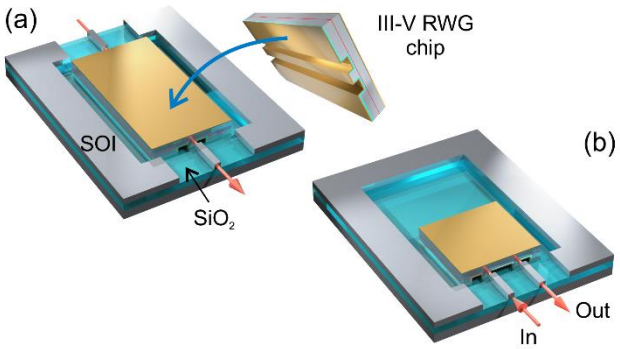

FIG 1. An illustration of the hybrid integration of III V chips on SOI-PIC. (a) A standard straight ridge-waveguide (RWG) III V chip requiring precise dimensions and alignment control at both ends. (b) A U-bend III V waveguide components with the I/O ports at one side of the chip; the length of the chip is also reduced to ~50% compared to standard design.

if the mode-size of the waveguide is matched, in order to attain low coupling losses, an alignment with sub-micrometer tolerances is required. High-end flip-chip bonders can achieve the submicron precision but a problem arises with the traditional TW-SOAs (and also with electro-absorption modulators) having the input on one side of the chip and the output on the opposite side. This geometry entails the simultaneous alignment of the waveguides at the two opposite facets, demanding the precise control of the length of the III-V die. Unfortunately, the standard cleaving accuracy of the III-V chip exhibits a dimensional control no better than ± 5 μm. Therefore, a significant amount of the chips from a production lot of TW-SOAs are either too long to fit in the recessed area on the SOI circuit or too short to allow for low coupling losses, resulting in a reduced fabrication yield. This problem becomes even more acute when using bars of devices with angled cleaving (required to avoid internal reflection), making the cleaving inaccuracy

even more pronounced in terms of size difference between the ends of the chip.

To solve these issues, we demonstrate a U-shaped waveguide geometry that supports all the benefits of a typical TW-SOA with the distinction that both the input and output ports of the chip are on the same side, as shown in Figure 1(b). Thus, the dicing accuracy is no longer a critical parameter influencing the yield or the optical losses, and the alignment monitoring for the flip-chip bonding must be ensured only at one edge of the die. Moreover, the spacing between the inputs and outputs is defined by lithography in accordance with the pitch between the silicon waveguides, achieving a coupling accuracy similar to heterogeneous and monolithic integration approaches.

The U-bend waveguide design follows the shape of the Euler spiral[4,5] to minimize bending losses, especially for the low radius bends that are required to maximize the integration density on a silicon circuit. Somewhat similar solutions to fabricate single-facet devices have been presented previously. For example, Yuan et al. utilized matched-arc bends[6] and Liang et al.[7] and Wang et al.[8] utilized wet oxidation to fabricate deep-etched high-index contrast (HIC) bends. Our approach is to use narrow waveguides targeting a wider operation bandwidth, larger tolerance to fabrication errors, and smaller size.

The U-bend device consists of two straight rib waveguide sections and a connecting ridge-waveguide bend defined by the two mirror-symmetric Euler spiral segments[4,9]. The geometry is shown in Figure 2. The bending radius decreases linearly as a function of the arc length, reaching its minimum at the apex. In the following discussion, we will be using the minimum bending radius as the defining characteristic of the bend, while also the effective bending radius can be calculated from the distance between the beginning and end of the bend. For U-bends, the effective bending radius is found to be 1.38 times the minimum bending radius[4]. Unlike the straight sections, the bent waveguide is etched all the way through the epitaxial layers including the n-side cladding layer to ensure higher lateral confinement[10, 11].

The epitaxial structure of the components comprises two InGaNAs quantum wells (QWs) surrounded by 318 nm thick

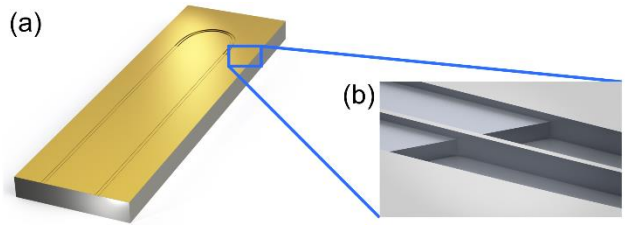

FIG 2. (a) The RWG devices with an Euler bend to bring the I/O channels on the same facet. (b) The bend area is etched deeper, through the active area to facilitate the better guiding of the mode through the bend.

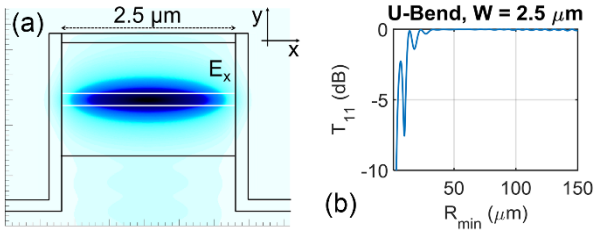

FIG 3. (a) The calculated fundamental mode profile of the waveguide (b) and the coupling to the fundamental mode at the output of the U-bend as a function of the minimum bending radius.

GaAs waveguide layers and 1 µm thick Al0.6Ga0.4As claddings. The SOA material was previously used in a straight waveguide TW design proving high-gain, un-cooled operation capabilities[12]. A suitable U-bend geometry was designed by varying the waveguide width (from 1.0 µm to 2.5 µm) and bend radius (from 1 µm to 200 µm) in a very efficient 3D simulation model based on a 2D mode expansion and tilted overlap integrals[5] predicting transmission through the whole bend. Modal simulations clearly show that the deeply etched bend waveguide is highly multimode in the horizontal direction. Complex mode solvers show that the modes of the straight waveguide, including the fundamental mode, are actually leaky modes, leaking in the high refractive index substrate. The calculated leaking loss is about 2 cm^{-1} (not including the absorption loss due to QWs and doping). Instead, the bends have been simulated using a real mode solver, therefore neglecting the imaginary part of the effective index, in order to extract the sole contribution of the bend to the overall losses. Indeed, the two sources of loss can be treated independently, given that neglected radiation losses are in the order of 0.5 dB, and can therefore be estimated using the perturbation theory. The simulations asserted that the mode guiding is possible only with a strongly confined mode profile, as presented in Figure 3 (a), requiring an index confinement on both n and p-side of the device. Figure 3 (b) displays the transmission as a function of the minimum bending radius of the Euler spiral shaped bend. The simulations show that after a certain critical radius of the bend, the transmission losses become negligible compared to the gain provided by the active material.

In order to estimate the transmission losses through the bend, a set of U-bend components with different lengths of straight RWG sections were prepared. The fabrication of the U-shaped RWG was done in two photolithography steps. First, a patterning was applied to define an etching mask for the straight and bent waveguides followed by a shallow etching through the p-cladding. In the second lithography step, the straight rib waveguide sections that do not require deep etching were protected with a photoresist and the etching was continued all the way through the n-side

cladding layer. The resulting shape of the waveguide is displayed in Figure 2 (b). After the formation of the waveguide, a layer of SiN_x was deposited on the surface and etched away from the top of the waveguide using a photolithography step. SiN_x provides mode guiding with a refractive index difference of $\Delta n \approx 1.1$. Subsequently the p-side of the substrate was metallized, the substrate thinned down to 110 µm in thickness and the n-metal layer deposited and annealed. For characterization purposes, the chips were diced perpendicular to the waveguide to form a semiconductor mirror facet at both ends of the U-bend, ensuring 28 % back-reflection due to the refractive index difference of $\Delta n \approx 2.4$ between the semiconductor and air. For the operation of the TW-SOA, these reflections are undesirable and typically avoided by dicing with a tilt and depositing anti-reflection coatings, but in this study we exploit them to extract both the gain characteristics and the bending losses of the resulting U-shaped laser resonator.

The analysis of the bend losses includes a comparison between straight waveguides and the U-bend geometry, in terms of the output power vs. current for devices operated as laser diodes. Following the standard derivation for the gain and loss characteristics of a straight Fabry-Perot laser diode[13], we assume the losses in the straight cavity to equal the threshold modal gain Γg_{th}

$$\boldsymbol{\Gamma g_{th} = \alpha_i + \alpha_m.} \quad (1)$$

The loss terms are the internal losses α_i and the mirror losses α_m. We assume that the internal loss term also contains the scattering losses caused by the sidewall roughness. Subsequently, the differential quantum efficiency η_d through the internal quantum efficiency η_i and the loss terms α_i and α_m is defined as:

$$\boldsymbol{\eta_d = \frac{\eta_i \alpha_m}{\alpha_i + \alpha_m}.} \quad (2)$$

The differential quantum efficiency of each component can be calculated directly from the slope efficiency of the of output power vs. drive current. For the U-bend device to operate as a laser diode, the gain and the losses have to be equal. However, we have to introduce an additional loss terms to account for the bend. Thus, we include into Eq. (1) the α_b term, accounting for the mode leaking from the curving waveguide, and the α_C term, accounting for the losses at the interface between the straight and bend sections

$$\boldsymbol{\Gamma g_{th} = \alpha_i + \alpha_m + \alpha_b + \alpha_c.} \quad (3)$$

If we replace the loss terms in the denominator of Eq. (2) with the ones in Eq. (3) and follow derivation in[13], we reach a linear equation with a slope-intercept form

$$\boldsymbol{\frac{1}{\eta_d} = \frac{\alpha_i + \alpha_b + \alpha_c}{\eta_i \, ln\left(\frac{1}{R}\right)} L + \frac{1}{\eta_i},} \quad (4)$$

where L is the length of the resonant cavity and R the facet power reflectivity. We also assume the modal gain to be the same for the straight and U-bend sections. To confirm the presence of gain in the bend section we operated devices with solely the U-bend structure as laser diodes and obtained lasing without a significant penalty; we thus conclude that the bend areas display gain characteristics, consequently at least partially justifying the assumption. For components without the bend, α_b and α_c are zero. From Eq. (4) we derive the slopes k_b and k_s for the U-bend and straight components, respectively, as:

$$\boldsymbol{k_s = \frac{\alpha_i}{\eta_i \, ln\left(\frac{1}{R}\right)}} \quad (5)$$

and

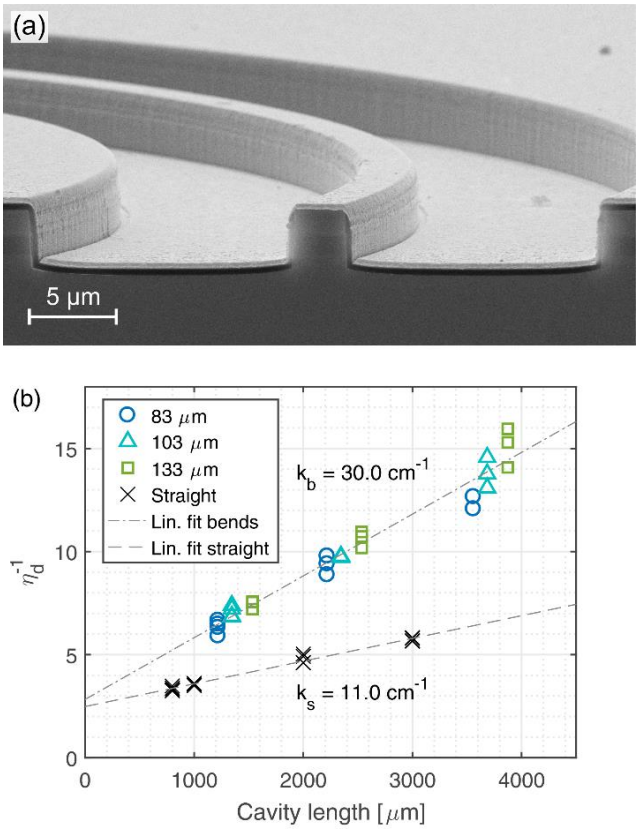

FIG 4. (a) Scanning electron microscope (SEM) image of the cross-section of the device at the bend area. (b) The inverses of the differential quantum efficiencies as a function of the total cavity length for Euler bend and straight RWG devices. For the bends, there are three different minimum radii of curvature used. From the linear fit, we can clearly see the deviation of the bend devices from the straight RWG. By using the slope value difference, we can estimate the bend losses.

$$k_b = \frac{\alpha_i + \alpha_b + \alpha_c}{\eta_i \, ln\left(\frac{1}{R}\right)}. \quad (6)$$

From the Eq. (5) and (6) we can then solve the bend losses

$$\alpha_b = (k_b - k_s)\eta_i ln\left(\frac{1}{R}\right) - \alpha_c. \quad (7)$$

The slope values can be obtained by plotting the measured values of $1/\eta_d$ as a function of L and making a linear fit to these data points.

To assess the coupling losses α_C we inspected the interface between the straight RWG and the U-bend. The step formed by the transition from shallow to deep etched ridge causes a change in the effective refractive index and in the mode shape of the waveguide, leading to reflections and mode mismatch at the interface, i.e. to additional losses. The transmittance and reflectance were simulated using the Eigen Mode Expansion (EME) method. The reflectance of the fundamental mode was estimated to be 3×10^{-4} and the coupling efficiency for the fundamental mode from rib to ridge waveguide 89.9 %, equaling a loss of 0.46 dB.

The component set studied contained straight and U-bend laser resonators with a RWG width of 2.5 µm and three different bend radius variations. Figure 4 (a) shows the device cross-section at the bend area. For the different variants, the total length of the straight sections were 700 µm, 1700 µm and 3040 µm with the lengths of the respective bend sections being 519 µm, 645 µm and 843 µm and the minimum radii of curvature being 83 µm, 103 µm and 133 µm, respectively. For comparison, a set of straight RWG devices with different cavity lengths of 800 µm, 1000 µm, 2000 µm and 3000 µm were prepared. The devices were operated in continuous wave (CW) mode as laser diodes at 20 °C and their light output powers were measured at different operating currents up to 200 mA. From the data, the internal quantum efficiency and the internal losses were calculated with the method described in[13] for the straight RWG cavities with the following results: $\eta_i = 0.4$ and $\alpha_i = 5.4$ cm^{-1}. The differential quantum efficiencies were calculated and their inverses plotted as a function of the total cavity length, as shown in Figure 4 (b). From the plot, we can clearly see the difference between the U-bend and straight RWG devices. The linear fits for the bend device and straight device plots give the distinctly different slope values of $k_b = 30.0$ cm^{-1} and $k_s = 11.0$ cm^{-1}, respectively. We estimate the bend losses to be on average 9.2 cm^{-1} by using the slope values in the Eq. (5). The calculations take the average over all different radii of curvature, since the bend losses do not seem to differ significantly across the different device variants. This indicates the possibility of further reducing the bending radii without an increase in the bend losses. For a bend with the radius of curvature of 83 µm and a bend length of 519 µm the bend loss for a single pass can be estimated to be about 1.1 dB, after subtracting the coupling loss of 0.9 dB from the two interfaces. The transition losses could be made negligible by designing a suitable adiabatic taper[14].

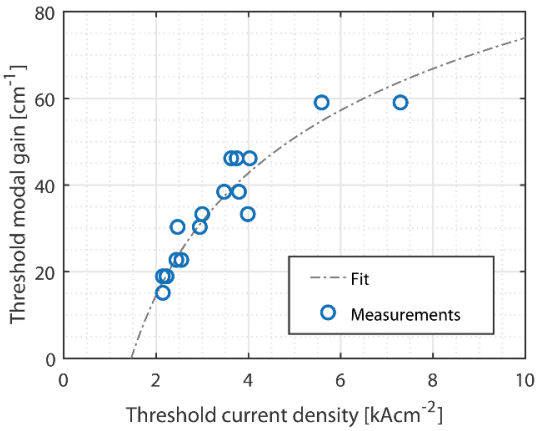

FIG 5. The gain of the waveguide vs the current density.

The gain characteristics of the devices were studied by comparing the threshold current densities of the straight RWG devices with the cavity lengths varying from 500 µm to 1500 µm and facet reflectivity of 28 % (as-cleaved) down to 2.1 %, which were obtained by applying antireflection coatings on the facets. The threshold current densities were compared with the gain required to overcome the internal and mirror losses at threshold current density. The results are plotted in Figure 5 and fitted to a logarithmic model derived from the gain-carrier density relation. The measurement results in the Figure 5 show that the waveguides are able to provide up to 60 cm^{-1} gain, significantly exceeding the measured bend losses.

In conclusion, we demonstrated a low loss U-bend waveguide exploiting the Euler spiral design to guide the light in a bent GaAs RWG region. With this approach, the I/O channels of the SOA can be positioned on the same facet of the device in order to significantly simplify the coupling to a SOI-platform. The modeling of the U-bend shows that for a III-V waveguide there is a threshold minimum bending radius that dictates the tightest bend still allowing nearly negligible bending losses. More specifically, we demonstrated the operation of the U-bends with a 2.5 µm wide ridge at 1.3 µm wavelength exhibiting as low as 9.2 cm^{-1} bend losses. For a U-bend device with the 83 µm bending radius this leads to a 1.1 dB bend loss. When we add the coupling losses from straight to bent waveguide of 0.9 dB, we obtained a total bend loss of 2.0 dB. Besides the advantages regarding the coupling, this approach enables an almost 50 % reduction in the length of the SOA chips required for achieving a particular gain value, thus enabling a higher integration density and better utilization of III-V materials. Similar benefits could be achieved by applying

the Euler bend design to electro-absorption modulators (EAM); for EAMs the size reduction could provide also benefits in terms of reduced parasitic and increased speed. The GaInNAs/GaAs waveguides enable operation also to 1.55 μm and bring known temperature behavior benefits.

The authors wish to acknowledge the help from Dr. Heikki Virtanen who provided the design for the rib waveguide. The work was funded by the EU FP7 project RAPIDO (Grant Agreement 619806) and the EU H2020 project MIREGAS (Grant Agreement 644192).

References

1 Z. Zhou, B. Yin, and J. Michel, Light Sci. Appl. 4, e358, (2015).

2 T. Alexoudi, D. Fitsios, G. T. Kanellos, N. Pleros, T. Tekin, M. Cherchi, S. Ylinen, M. Harjanne, M. Kapulainen, and T. Aalto, SPIE Photonics West 2014-OPTO Optoelectron. Devices Mater. 8990, 89900N (2014).

3 M. Kapulainen, S. Ylinen, T. Aalto, M. Harjanne, K. Solehmainen, J. Ollila, and V. Vilokkinen, in 2008 5th IEEE International Conference on Group IV Photonics, 61 (IEEE, 2008).

4 M. Cherchi, S. Ylinen, M. Harjanne, M. Kapulainen, and T. Aalto, Opt. Express 21, 17814, (2013).

5 M. Cherchi, S. Ylinen, M. Harjanne, M. Kapulainen, T. Vehmas, and T. Aalto, Proc. SPIE 8990, 899004, (2014).

6 W. Yuan, C. S. Seibert, and D. C. Hall, IEEE J. Sel. Top. Quantum Electron. 17, 1662 (2011).

7 J. Wang, W. Yuan, C. S. Seibert, and D. C. Hall, in Proc. SPIE 7230, Novel In-Plane Semiconductor Lasers VIII, 72300J (2009).

8 D. Liang, J. Wang, and D. C. Hall, IEEE Photonics Technol. Lett. 19, 598, (2007).

9 D. S. Meek and D. J. Walton, J. Comput. Appl. Math. 25, 69 (1989).

10 D. Liang, J. Wang, J. Yu-Ting Huang, J.-Y. Yeh, L. J. Mawst, and D. C. Hall, IEEE J. Sel. Top. Quantum Electron. 13, 1324, (2007).

11 M.-K. Chin, C.-W. Lee, S.-Y. Lee, and S. Darmawan, Appl. Opt. 44, 3077 (2005).

12 D. Fitsios, G. Giannoulis, V.-M. Korpijärvi, J. Viheriälä, A. Laakso, N. Iliadis, S. Dris, M. Spyropoulou, H. Avramopoulos, G. T. Kanellos, N. Pleros, and M. Guina, Appl. Opt. 54, 46 (2015).

13 L. A. Coldren, S. W. Corzine, and M. Mashanovitch, Wiley, 2nd ed., 45 (2012).

14 T. Aalto, K. Solehmainen, M. Harjanne, M. Kapulainen, and P. Heimala, IEEE Photonics Technol. Lett. 18, 709 (2006).